

# Rapid computation of photoacoustic fields from normal and pathological red blood cells using a Green's function method

Ratan K. Saha<sup>a</sup>, Muhammad N. Fadhel<sup>b</sup>, Aamna Lawrence<sup>a</sup>, Subhajit Karmakar<sup>c</sup>, Arunabha Adhikari<sup>d</sup>, and Michael C. Kolios<sup>b</sup>

<sup>a</sup>Department of Applied Sciences, Indian Institute of Information Technology Allahabad, Allahabad, India

<sup>b</sup>Department of Physics, Ryerson University, Toronto, Canada; Li Ka Shing Knowledge Institute/Keenan Research Center, St. Michaels Hospital, Toronto, Canada

<sup>c</sup>University Science Instrumentation Centre, The University of Burdwan, Bardhaman, India

<sup>d</sup>Department of Physics, West Bengal State University, Berunanpukuria, India

## ABSTRACT

Photoacoustic (PA) field calculations using a Green's function approach is presented. The method has been applied to predict PA spectra generated by normal (discocyte) and pathological (stomatocyte) red blood cells (RBCs). The contours of normal and pathological RBCs were generated by employing a popular parametric model and accordingly, fitted with the Legendre polynomial expansions for surface parametrization. The first frequency minimum of theoretical PA spectrum approximately appears at 607 MHz for a discocyte and 410 MHz for a stomatocyte when computed from the direction of symmetry axis. The same feature occurs nearly at 247 and 331 MHz, respectively, for those particles when measured along the perpendicular direction. The average experimental spectrum for normal RBCs is found to be flat over a bandwidth of 150-500 MHz when measured along the direction of symmetry axis. For spherical RBCs, both the theoretical and experimental spectra demonstrate negative slope over a bandwidth of 250-500 MHz. Using the Green's function method discussed, it may be possible to rapidly characterize cellular morphology from single-particle PA spectra.

**Keywords:** Photoacoustics, Erythrocyte, Stomatocyte, Green's function, Legendre polynomial

## 1. INTRODUCTION

A normal red blood cell (RBC) under physiological conditions looks to be a biconcave discoid (discocyte). However, researchers have found that there are many agents that can modify RBC morphology leading to axisymmetric and nonaxisymmetric shapes.<sup>1,2</sup> For example, some agents can induce a series of crenated RBC shapes known as echinocytes. Many equally spaced similar little protrusions projecting outwards are observed. On the other hand, there are several agents that can promote concave shapes referred to as stomatocytes. These are pathological shapes which may cause circulatory disorders. Most existing methods determining shapes of individual RBCs are laborious and time consuming.<sup>3</sup> Therefore, there is a need to develop a simple and fast technique for *in vitro* and *in vivo* characterization of RBC morphology.

Recent experimental studies demonstrate that it may be feasible to examine RBC morphology using the photoacoustic (PA) technique.<sup>3-6</sup> In these works, an erythrocyte is illuminated with a 532 nm laser beam and the generated acoustic signal is detected using ultra-high frequency transducers operating at hundreds of MHz. PA spectral features for a nonspherical cell are found to be different when probed from different directions. Moreover, measured spectra exhibit variation when cells of different shapes are investigated. The size and shape dependent spectral signatures may help to quantify cellular morphology with PAs.

In this work, we first made an attempt to theoretically produce PA spectra from normal (discocyte) and pathological (stomatocyte) RBCs. The pressure fields for such cells were computed by solving the PA wave equation using a Green's function approach.<sup>7</sup> This method can be employed to calculate PA fields from irregular

---

Further author information: ratank.saha@iitaa.ac.in, Telephone: 91 532 292 2417

objects at frequencies higher than 100 MHz, where the shape of micron-sized particles (e.g. RBCs) impacts the spectral domain at high frequencies.<sup>3</sup> The Legendre polynomial expansions were used to fit the boundaries of normal and pathological RBCs for surface parameterization. We also conducted experiment to measure single cell PA spectrum for comparison. Experimental and theoretical results exhibit similar trends.

The layout of the paper is as follows. Section 2 presents the mathematical derivation of the PA field. The parametric models (e.g. Evans and Fung model, Kuchel and Fackerell model) for constructing RBC contour are also illustrated in this section. Various numerical parameters considered during PA field calculation, RBC contour fitting, experimental set up, sample preparation and signal analysis are briefly described in Section 3. In section 4, numerical and experimental results are provided. The discussion and conclusions of this study are given in section 5.

## 2. MATHEMATICAL ANALYSIS

### 2.1 PA pressure derivation

The time independent wave equation for PA pressure ( $p$ ) is given by,<sup>8,9</sup>

$$\nabla^2 p + k^2 p = \begin{cases} \frac{i\omega\mu_a\beta I_0}{C_P}, & \text{inside the absorber} \\ 0, & \text{outside the absorber.} \end{cases} \quad (1)$$

where  $\mu_a, \beta, C_P$  constitute the optical absorption coefficient, isobaric thermal expansion coefficient and specific heat of the absorbing region, respectively. The modulation frequency and intensity of the incoming light beam are represented by  $\omega$  and  $I_0$ , whereas  $k$  signifies the wavenumber of the outgoing sound waves. In deriving Eq. (1), the conditions of thermal and stress confinement are imposed. Further, the acoustic characteristics inside the PA source and its surroundings are assumed to be identical. The solution to Eq. (1) can be written as,<sup>10</sup>

$$p_{\text{ext}}(\mathbf{r}, k) = - \int A G(\mathbf{r}|\mathbf{r}_0) d^3\mathbf{r}_0, \quad (2)$$

where  $A = \frac{i\omega\mu_a\beta I_0}{C_P}$  and  $G(\mathbf{r}|\mathbf{r}_0)$  defines the free space Green's function. Here,  $\mathbf{r}$  and  $\mathbf{r}_0$  are the field and source points, respectively. The subscript ext is used to express the pressure field outside the absorbing region (i.e.  $r > r_0$ ). The PA geometry is shown in Fig. 1. The Green's function can be expressed as,<sup>10</sup>

$$G(\mathbf{r}|\mathbf{r}_0) = \frac{e^{ik|\mathbf{r}-\mathbf{r}_0|}}{4\pi|\mathbf{r}-\mathbf{r}_0|}. \quad (3)$$

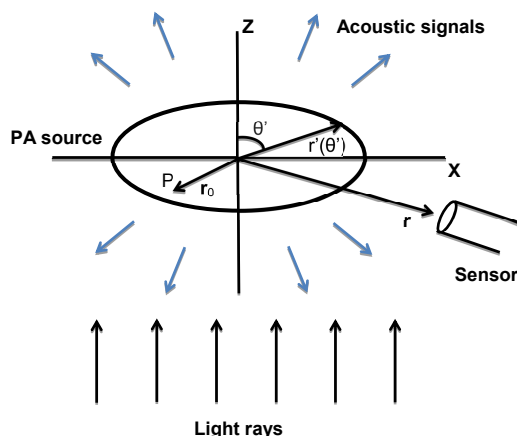


Figure 1. The PA geometry.

When  $r \gg r_0$  with  $\mathbf{k}$  as the wave vector in the direction of the detector, Eq. (2) can be simplified as,

$$p_{\text{ext}}(\mathbf{r}, k) \approx -\frac{e^{ikr}}{4\pi r} \int A e^{-i\mathbf{k}\cdot\mathbf{r}_0} d^3\mathbf{r}_0 = \frac{e^{ikr}}{r} M(\mathbf{k}), \quad (4)$$

where  $M(\mathbf{k})$  is given by,

$$M(\mathbf{k}) = -\frac{1}{4\pi} \int A e^{-i\mathbf{k}\cdot\mathbf{r}_0} d^3\mathbf{r}_0. \quad (5)$$

Eq. (5) for a homogeneous axisymmetric PA source becomes,

$$M(\mathbf{k}) = -\frac{A}{4\pi} \int_0^\pi \sin\theta_0 d\theta_0 \int_0^{F(\theta_0)} r_0^2 dr_0 \int_0^{2\pi} e^{-i\mathbf{k}\cdot\mathbf{r}_0} d\phi_0. \quad (6)$$

Here, the geometry of an irregular absorber is described in spherical polar coordinates  $(r', \theta', \phi')$  by setting  $r' = F(\theta')$  where  $F$  is a function that relates  $r'$  and  $\theta'$  (see Fig. 1). In this work, pressure fields from RBCs having azimuthal symmetry have been computed by performing the integration of the above equation.

## 2.2 RBC contour determination

Many mathematical models have been developed to mathematically describe the RBC contour. The most widely used being the Evans and Fung model is given by the equation,<sup>11</sup>

$$z(u) = \sqrt{1 - \left(\frac{u}{R}\right)^2} \left[ c_0 + c_1 + c_2 \left(\frac{u}{R}\right)^2 \right], \quad (7)$$

where  $u$  is the horizontal distance and  $c_0$ ,  $c_1$  and  $c_2$  are the empirical constants that determine the shape of RBC. Another popular model for constructing the RBC contour was proposed by Kuchel and Fackerell.<sup>12</sup> It has three parameters namely  $\xi_1$ ,  $\xi_2$  and  $\xi_3$  that determine the RBC shape and is represented by the following equation:

$$(u^2 + z^2)^2 + \xi_1 u^2 + \xi_2 z^2 + \xi_3 = 0. \quad (8)$$

The coefficients  $(c_0, c_1, c_2$  or  $\xi_1, \xi_2, \xi_3)$  can be determined from four morphological parameters.<sup>13</sup> These parameters are the diameter ( $D = 2R$ ), dimple thickness ( $t$ ), maximum thickness ( $h$ ) and the diameter drawn on the location of maximum height ( $d$ ). The coefficients of Eq. (7) and Eq. (8) can be solved by constructing three equations using boundary conditions. For the Kuchel and Fackerell model, these can be illustrated as follows.

Case 1: At  $u = 0$  and  $z = t/2$ , we get,

$$(t/2)^4 + \xi_2(t/2)^2 + \xi_3 = 0. \quad (9)$$

Case 2: At  $u = d/2$  and  $z = h/2$ , we obtain,

$$((d/2)^2 + (h/2)^2)^2 + \xi_1(d/2)^2 + \xi_2(h/2)^2 + \xi_3 = 0. \quad (10)$$

Case 3: At  $u = R$  and  $z = 0$ , the equation becomes,

$$R^4 + \xi_1 R^2 + \xi_3 = 0. \quad (11)$$

Eqs. (9), (10) and (11) in this work were used to evaluate the coefficients. The contours generated for a normal RBC as well as pathological RBCs (referred to as the Stomatocyte1 and Stomatocyte2 in the text) were generated using the Kuchel Fackerell parametric equation and are shown in Fig. 2. For the stomatocytes, the upper hemisphere was constructed using the Eq. (8) whereas the lower half was considered as a half sphere. The morphological parameters that govern the shape of the normal and pathological RBCs are given in Table 1.

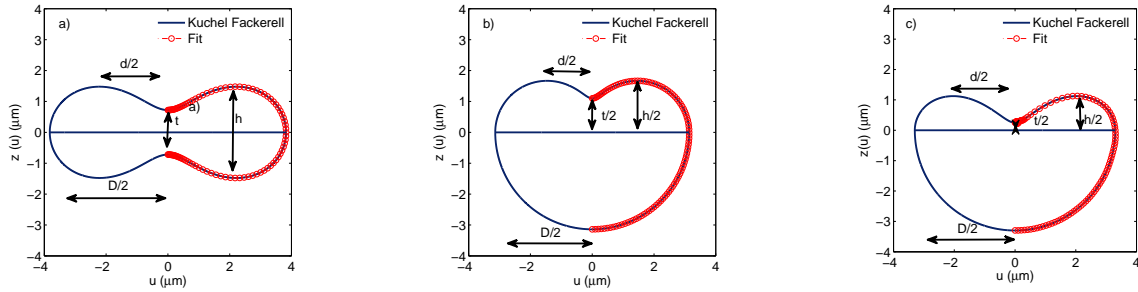


Figure 2. Two-dimensional cross-sections of normal and pathological RBCs. (a) Normal RBC, (b) Stomatocyte1, (c) Stomatocyte2.

Table 1. Numerical values of various parameters used to simulate the shapes of normal and pathological RBCs.

Cell type	Volume ( $\mu\text{m}^3$ )	D ( $\mu\text{m}$ )	$t/2$ ( $\mu\text{m}$ )	$h/2$ ( $\mu\text{m}$ )	R ( $\mu\text{m}$ )	d ( $\mu\text{m}$ )	L
Discocyte	108.5	7.65	0.72	1.42	D/2	0.7D	19
Stomatocyte1	105.8	6.28	1.1	1.5	D/2	0.7D	19
Stomatocyte2	105.7	6.60	0.25	1.1	D/2	0.7D	19

### 3. MATERIALS AND METHODS

#### 3.1 Numerical specification

##### 3.1.1 Physical parameters

The density and the velocity used in the modeling are  $\rho = 1005 \text{ kg/m}^3$  and  $v = 1500 \text{ m/s}$ , respectively for both the PA source and the surrounding medium. Optical and thermomechanical parameters for the PA source were given fixed values ( $I_0 = 1$ ,  $\mu = 1$ ,  $\beta = 1$ ,  $C_P = 1$ ) as we are interested only in spectral features. Note that these parameters control the amplitude of the PA signal and do not change its spectral content. The computation for the PA pressure amplitude was done for a frequency range of 1.5 to 2000 MHz. To determine the integral in Eq. (6), the volume of the PA source was divided into cubic voxels of 200 nm length. A built-in function in MATLAB called trapz was used to perform numerical integration based on the trapezoidal rule. All computations were performed on a personal computer having Intel(R) Core(TM) i7-5500U CPU working at 2.4 GHz and having 16 GB RAM.

##### 3.1.2 RBC contour parameters

The theoretically constructed contours of the normal and pathological RBCs were fitted (see Fig. 2) with the Legendre polynomial expansions for surface parameterization such as:<sup>7</sup>

$$r'(\theta') = R[1 + \sum_n \alpha_n P_n(\cos \theta')]. \quad (12)$$

To accomplish this, a number of radial samples (i.e.  $r_1, r_2, \dots, r_s$ ) at different angular locations ( $\theta_1, \theta_2, \dots, \theta_s$ ) were computed using Eq. (8). A system of equations was then constructed by considering the Legendre polynomials of degree  $L$  and could be presented as,

$$\begin{pmatrix} P_0(\cos \theta_1) & P_1(\cos \theta_1) & \dots & P_L(\cos \theta_1) \\ P_0(\cos \theta_2) & P_1(\cos \theta_2) & \dots & P_L(\cos \theta_2) \\ \vdots & \vdots & \dots & \vdots \\ P_0(\cos \theta_s) & P_1(\cos \theta_s) & \dots & P_L(\cos \theta_s) \end{pmatrix} \begin{pmatrix} \alpha_0 \\ \alpha_1 \\ \vdots \\ \alpha_L \end{pmatrix} = \begin{pmatrix} r_1/R_e - 1 \\ r_2/R_e - 1 \\ \vdots \\ r_s/R_e - 1 \end{pmatrix}. \quad (13)$$

In this paper,  $s = 100$  radial samples were taken and the Legendre polynomial up to degree  $L = 19$  was taken.<sup>14</sup> This set of equations were solved using the least square fitting technique to obtain the  $\alpha$  vector. Plots of  $\alpha$

vectors for discocyte, Stomatocyte1 and Stomatocyte2 are shown in Fig. 3. It demonstrates that  $\alpha$  vectors are different for different shapes and therefore, can be used to quantify cellular morphology.

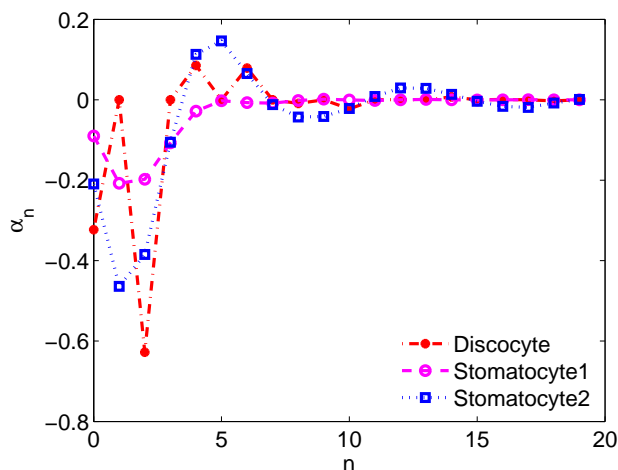


Figure 3. Plots of coefficients ( $\alpha_n$ ) of the Legendre polynomials that constitute the  $\alpha$  vectors.

## 3.2 Experiments

### 3.2.1 Experimental set up

A customized PA microscope was used to obtain the radio frequency (RF) signals emitted by normal and "spherical" RBCs. The experimental set up consists of an ultrasound transducer, laser and an optical microscope<sup>3-5, 15</sup> (see Fig. 4). The center frequency of the ultrasound transducer (Kibero GmbH, DE) used for the analysis was 340 MHz. In addition to the above, a laser (Teem Photonics, FR) having a pulse length of 330 picoseconds (ps) was used so that the conditions of the stress and thermal constraint were met for RBCs. For focusing the laser on the RBCs, an optical microscope was used having a 10x objective lens that could focus the laser on a 10  $\mu$ m spot. The entire set up was placed in a chamber whose temperature was maintained at 37°C.

### 3.2.2 Sample preparation and signal collection

Under protocol #2015-203 of Ryerson University Ethics protocol, blood samples for analysis from healthy individuals were obtained from the Canadian blood services. Spherical RBCs were prepared by mixing 50 mU/ml SMase to the biconcave RBCs.<sup>16</sup> The blood samples were diluted with Dulbeccos modified Eagles Medial (DMEM) and

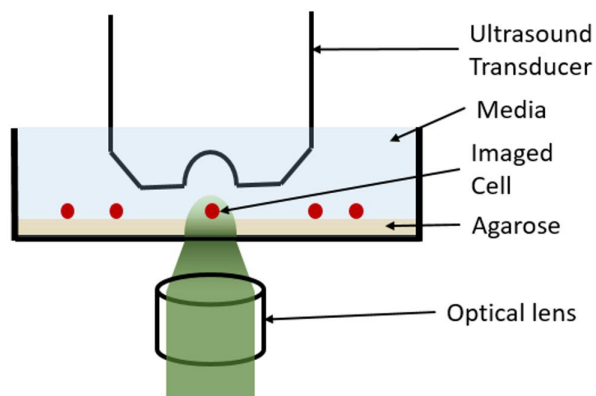


Figure 4. Schematic representation of the experimental set up.

10% fetal bovine serum (FBS) in the ratio 1:250. In a petri dish (Mattek Corporation USA) containing 1 ml of 1% agarose (Sigma Aldrich, CA), the blood specimens were fixed to reduce reflection from the sample holder.<sup>5</sup> The RF signals generated by the RBCs were recorded using the high frequency ultrasound transducer. A 25 ns sized Hann window was used to isolate the RBC signal and to generate the power spectra of the RF signals. The power spectra were obtained for 25 normal and spherical RBCs and normalized to the power spectra of 20 nm thick gold film that was used as a reference to suppress the system dependent effects. The spectra of the experimental and theoretical prototype were then compared.

## 4. RESULTS

### 4.0.1 Numerical result

The plots of  $|M(f)|^2$  for a discocyte, Stomatocyte1 and Stomatocyte2 are given in Fig. 5 for two detector locations ( $\theta = 0$  and  $\frac{\pi}{2}$  relative to the Z axis, see Fig. 1). The same plot for a sphere (black line) is also provided in this figure for comparison. The first spectral minimum for a normal RBC occurs at approximately 607.5 MHz. Since the RBC is very thin in the direction of  $\theta = 0$ , the first minimum appears at a very high frequency. The first minimum for Stomatocyte1 appears nearly at 409.5 MHz and for Stomatocyte2 it is close to 436.5 MHz. These spectral shifts may be attributed to the fact that stomatocytes are much thicker than normal RBC along the symmetry axis. The first minimum for the discocyte is further shifted to a lower frequency (approximately at 247 MHz) when probed from  $\theta = \pi/2$ . Similar observations can be made for stomatocytes ( $\approx 331.5, 310.5$

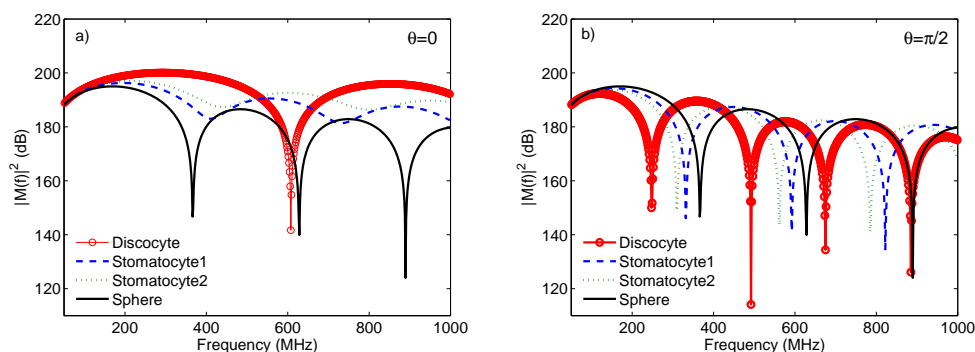


Figure 5. Computed  $|M(f)|^2$  for normal and pathological RBCs as a function of frequency. (a) The quantity is evaluated at  $\theta = 0$  direction. (b) Same as (a) but for  $\theta = \frac{\pi}{2}$ .

MHz, respectively). Since for a sphere the aspect ratio remains the same in all directions, the first minimum in the spectrum at  $\theta = 0$  and  $\theta = \pi/2$  occurs at about 366 MHz.

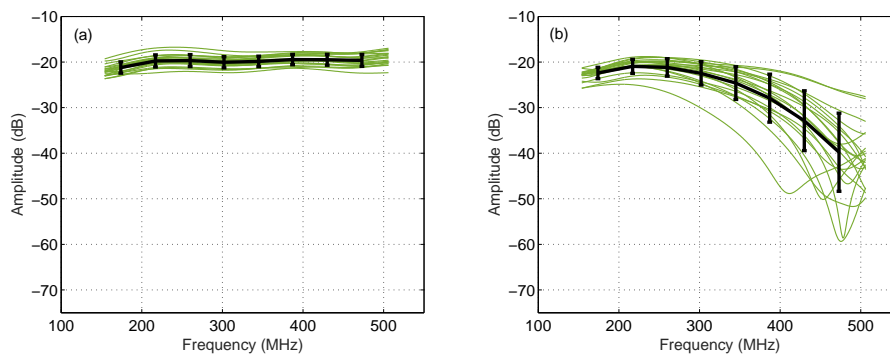


Figure 6. Spectral plots of windowed radio frequency photoacoustic signals. (a) Spectral plot of 25 biconcave red blood cells. (b) Spectral plot of 25 spherical red blood cells exposed to SMase.

#### 4.0.2 Experimental result

The measured spectra along the direction  $\theta = 0$  for normal RBCs are presented in Fig. 6(a). The same curves for SMase exposed RBCs are shown in Fig. 6(b). The average spectrum for normal RBC is flat (featureless) over the ultrasound detector bandwidth. However, for the spherical RBC, amplitude of the mean curve decreases as the frequency increases. This trend can be seen at frequency above 250 MHz. The spectral amplitude becomes minimum at approximately 470 MHz.

### 5. DISCUSSIONS AND CONCLUSIONS

A comparison between the theoretical and the experimental findings are presented in Fig. 7. It clearly shows that the theoretical curve agrees well with the measured values for normal RBCs within the bandwidth of 175-375 MHz ( $\theta = 0$ ). For pathological case, the experimental curve (cyan line) demonstrates close match with the Stomatocyte2 line but deviates from the spherical RBC data. Grossly, there is a strong agreement between the theoretical and the experimental trends for both normal and pathological RBCs.

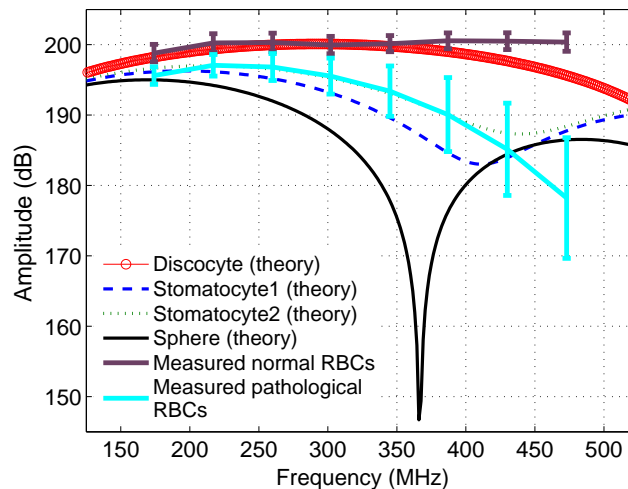


Figure 7. Comparison between theoretical and experimental spectral curves (normalized).

Theoretical spectra pass through successive maxima and minima (see Fig. 5). It is known that this peak and trough pattern depends upon the size of the particle along the direction of measurement. The position of the first minimum for a normal RBC is found to be at 607 MHz when computed along the symmetry axis. The corresponding average experimental spectrum is flat over the measurement bandwidth (150-500 MHz) and does not show any dips (see Fig. 6(a)). This is expected because the average width (along  $\theta = 0$ ) of normal RBCs is small and the first minimum might have occurred above the detection bandwidth. Similarly, locations of the first minimum are computed to be at 366 and 470 MHz, respectively, from the theoretical and experimental curves for spherical particles. It could also be speculated that the spherical particle considered in the theory was thicker than the experimental particle. However, additional microscopic and PA measurements are required for confirmation.

Different parametric models (e.g. Evans and Fung model and Kuchel and Fackerell model) for generating RBC contour were discussed in this work. These models provide axisymmetric shapes which can be fitted with the Legendre polynomial expansions. In future it would be interesting to produce nonaxisymmetric shapes using spherical harmonics expansions and accordingly, study PA response of such particles. Further, in future, confocal microscopy may be used to generate realistic nonsymmetric shapes.

In conclusion, a simple Green's function approach for calculating PA spectrum for an object is discussed. It can predict the PA spectrum of a source of arbitrary shape. The PA spectra from normal and pathological



RBCs have been generated using this approach. It is found that the width of the source along the direction of measurement dictates the spectral pattern. Both the theoretical and experimental spectra for normal RBC remain flat within a bandwidth of 150-500 MHz when measured along the symmetry axis. The spectral slopes for theoretical and experimental curves are found to be negative within a bandwidth of 250-500 MHz for spherical RBCs. The theoretical spectrum can be rapidly calculated using the Green's function method and such a spectrum may be used to fit an experimental spectrum for evaluating cellular size in realistic time frames.

## ACKNOWLEDGMENTS

RKS would like to express his gratitude to late Prof. Binayak Dutta-Roy of Saha Institute of Nuclear Physics for introducing how to an axisymmetric shape could be fitted with the Legendre polynomial expansion. The financial supports from the Department of Science and Technology, New Delhi; IIIT Allahabad; and the Natural Sciences and Engineering Research Council of Canada/Canadian Institutes of Health Research (Collaborative Health Research Projects grant number 462315-2014) are also gratefully acknowledged.

## REFERENCES

- [1] Lim H W G, Wortis M and Mukhopadhyay R 2002 Stomatocyte-discocyte-echinocyte sequence of the human red blood cell: Evidence for the bilayer-couple hypothesis from membrane mechanics *PNAS* **99** 16766-16769.
- [2] Reinhart W H and Chien S 1986 Red cell rheology in stomatocyte-echinocyte transformation roles of cell geometry and cell shape, *Blood* **67** 1110-1118.
- [3] Strohm E M, Berndl E S L and Kolios M C 2013 Probing red blood cell morphology using high frequency photoacoustics *Biophys. J.* **105** 59-67.
- [4] Strohm E M, Berndl E S L and Kolios M C 2013 High frequency label-free photoacoustic microscopy of single cells *Photoacoustics* **1** 49-53.
- [5] Strohm E M, Gorelikov I, Matsuura N, and Kolios M C 2014 Modeling photoacoustic spectral features of micron-sized particles *Phys. Med. Biol.* **59** 5795-5810.
- [6] Moore M J, Strohm E M and Kolios M C 2016 Assessment of the nucleus-to-cytoplasmic ratio in MCF-7 cells using ultrahigh frequency ultrasound and photoacoustics *Int. J. Thermophys.* **37** 118.
- [7] Saha R K, Karmakar S, Adhikari A and Kolios M C Photoacoustic field calculation for nonspherical axisymmetric fluid particles *Biomed. Phys. Eng. Express* (in press).
- [8] Diebold G J, Sun T and Khan M I 1991 Photoacoustic monopole radiation in one, two and three dimensions *Phys. Rev. Lett.* **67** 3384-7.
- [9] Saha R K and Kolios M C 2011 A simulation study on photoacoustic signals from red blood cells *J. Acoust. Soc. Am.* **129** 2935-43.
- [10] Morse P M and Ingard K U 1968 *Theoretical Acoustics*(New York: McGraw-Hill) ch 7, pp 306-99.
- [11] Evans E and Fung Y C 1972 Improved measurements of the Erythrocyte geometry *Microvasc. Res.* **4** 335-47.
- [12] Kuchel P W and Fackerell E D 1999 Parametric-equation representation of biconcave erythrocytes *Bull. Math. Biol.* **61** 209-220.
- [13] Bi L and Yang P 2013 Modeling of light scattering by biconcave and deformed red blood cells with the invariant imbedding  $T$ -matrix method *J. Biomed. Opt.* **18** 055001.
- [14] Khairy K, Foo J and Howard J 2010 Shapes of red blood cells: comparison of 3D confocal images with the bilayer-couple model *Cell Mol. Bioeng.* **1** 173-81.
- [15] Strohm E M and Kolios M C 2011 Sound velocity and attenuation measurements of perfluorocarbon liquids using photoacoustic methods *2011 IEEE International Ultrasonics Symposium (IUS)* 2368-2371.
- [16] Fadhel M N, Strohm E M, and Kolios M C 2016 High frequency photoacoustic spectral analysis of erythrocyte programmed cell death (eryptosis) *2016 IEEE International Ultrasonics Symposium (IUS)* 1-4.